Chapter 2

Tribology of Slip Surfaces in Journal Bearings

Qiyin Lin, Baotong Li and Hong Zhao

Additional information is available at the end of the chapter

http://dx.doi.org/10.5772/63532

Abstract

Boundary slip can be triggered by certain engineered surfaces. Journal bearings with slip surfaces have markedly different performances compared with traditional journal bearings. In order to reasonably utilise boundary slip to improve the tribological performances of journal bearings, including hydrodynamic and hybrid journal bearings, it is necessary to draw out the impact laws of boundary slip on the performances of journal bearings. The design criterion of slip surfaces is presented in this chapter; only a well-designed slip surface could improve the tribological performances of journal bearings. This chapter could provide a valuable guide for the design of slip surfaces in journal bearings.

Keywords: boundary slip, journal bearing, tribological performance, impact law, design criterion

1. Introduction

Tribological performances of lubricated contacts are strongly governed by the boundary conditions of fluid flows that provide lubrication. Traditional textbooks always assume that the immediate layer of liquid next to a solid surface moves with the same tangential velocity as the solid surface itself, which is the well-known 'no-slip' assumption; but for over a century, there have been persistent doubts about its validity.

In recent years, a number of experiments have shown that for certain engineered surfaces, the no-slip boundary condition is not a valid one, and boundary slip might occur at the fluid-solid interface [1–3]. Such slip surfaces can be obtained by modifying the geometrical micro- or nanostructure of the surfaces and controlling the surface energy. The micro- or nanostructured patterns on solid surfaces can be created using micro-nano fabrication techniques such as plasma etching, lithographic techniques, electro chemical etching, laser texturing and so on.

And the surface energy of a solid surface can be controlled by such techniques as film or molecule deposition, solution coating, or self-assembly of hydrophobic layers.

A large number of literatures reported that the boundary slip phenomenon is very obvious and remarkable when liquids flow over superhydrophobic surfaces (not-wettable surfaces). It is remarkable that when boundary slip is introduced into lubricated contacts, their tribological performances would present significant differences comparing with that without slip [4–7]. Slip surfaces will significantly influence the tribological performances of lubricated contacts [5–12]. Thus, it is necessary and valuable to draw out these changes and differences with and without boundary slip. This chapter will look into the tribology of slip surfaces in journal bearings and reveal their impact laws on the tribological performances of hydrodynamic and hybrid journal bearings.

2. Slip numerical models

Nowadays, there are mainly three numerical models to describe the boundary slip phenomenon, i.e. slip length model, limiting shear stress slip model and slip intensity model.

The slip length model, also named Navier slip model, states that the slip velocity, U_s, is proportional to the surface shear rate, $\partial u/\partial y$, and slip length, b, seeing Eq. (1).

$$U_s = b \cdot \frac{\partial u}{\partial y} \tag{1}$$

The slip length, b, is defined as the fictive distance below the solid surface where the velocity extrapolates linearly to zero, as shown in **Figure 1**.

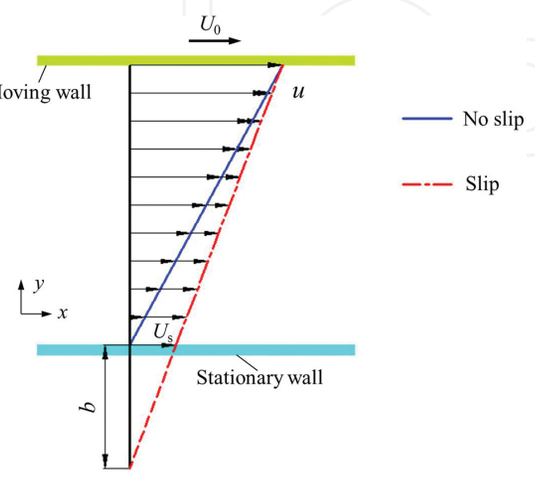

Figure 1. Slip length model.

The limiting shear stress slip model assumes that there is a critical shear stress, τ_c, at the fluid-solid interface and the wall slip occurs only when the wall shear stress, τ_0, reaches the critical value, τ_c. If slippage occurs, the surface shear stress, τ_s, is equal to the critical value, i.e.

$$\tau_s = \tau_c \quad (\tau_0 \geq \tau_c)$$

and others,

$$\tau_s = \tau_0 \quad (\tau_0 < \tau_c)$$

where

$$\tau_0 = \mu \cdot \frac{\partial u}{\partial y}$$

The reported slip length, b, ranges from the order of the mean free path of fluid molecular to micrometer, even centimeter; the reported critical shear stress, τ_c, still exists in an over-broad range; consequently, it is difficult to qualify the exacting value of slip length and critical shear stress.

Not only the slip length model but also the limiting shear stress slip model indicates that the slip velocity, U_s, is always related to fluid velocity, U_i, at the nearest region close to this fluid-solid interface. For the convenience, to determine the slip intensity, a slip-intensity factor, γ, is introduced and restricted from 0 to 1, which seems to be much easier to qualify, and the slip intensity increases with the value of slip-intensity factor, γ; thus, a slip intensity model is derived from the limiting shear stress slip model then and is expressed as

$$U_s = \gamma \cdot (U_i - n \cdot < U_i \cdot n >) \tag{2}$$

where n is the surface normal vector; the dot produce, $U_i \cdot n$, is the projection value of fluid velocity, U_i, projecting to the surface normal direction; the minus sign, –, in the formula represents that the angle between the surface normal vector, n, and the velocity vector, U_i, is an obtuse angle; and the dot produce, $n \cdot <U_i \cdot n>$, represents the velocity component of, U_i, in the surface normal direction.

Assuming that the three components of slip velocity, U_s, are u_s, v_s, w_s, and those three components of fluid velocity, U_i, are u_i, v_i, w_i, respectively, under the coordinate system x_n-y_n-z_n, where the direction of surface normal vector n is -z_n, as shown in **Figure 2**, Eq. (2) can be rewritten as

$$\begin{cases} u_s = \gamma \cdot u_i \\ v_s = \gamma \cdot v_i \\ w_s = 0 \end{cases}$$

Consequently, the slip intensity model indicates that the boundary slip only occurs in the tangential direction. When $\gamma = 1$, this slip model becomes the limiting shear stress slip model with $\tau_c = 0$, i.e. a shear free condition, also called perfect slip condition. When $\gamma = 0$, this slip model regresses to a no-slip boundary condition with zero velocity (stationary wall). For the convenience to identify the slip intensity and analyse its influences on the performances of journal bearings, the slip intensity model is utilised to represent the boundary slip in this chapter.

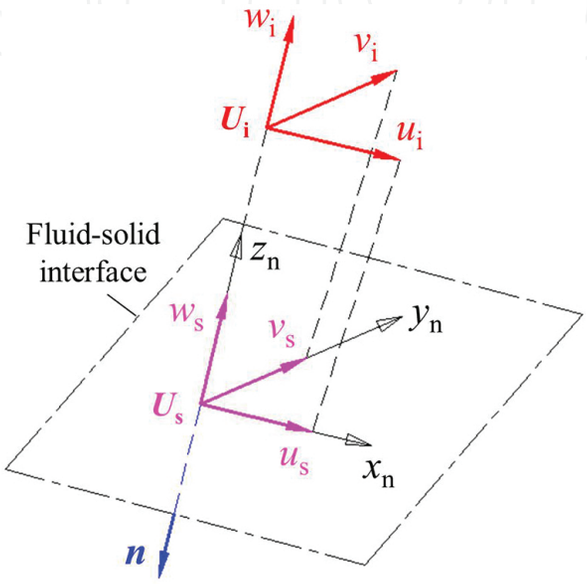

Figure 2. Schematic diagram of velocity.

3. Governing equations and cavitation model

In order to reduce the generation of frictional heat in high-speed journal bearing systems, lubricant with low-viscosity, such as water, is usually utilised, and water is chosen as the lubricant in this chapter. Assuming that water is a continuous isoviscous incompressible fluid medium, so continuity equation and full Navier–Stokes equations are used to predict the performances of the fluid domain. For steady-state study, these governing equations are expressed as

$$\frac{\partial u}{\partial x} + \frac{\partial v}{\partial y} + \frac{\partial w}{\partial z} = 0 \tag{3}$$

$$\rho\left(u\frac{\partial u}{\partial x} + v\frac{\partial u}{\partial y} + w\frac{\partial u}{\partial z}\right) = -\frac{\partial p}{\partial x} + \mu\left(\frac{\partial^2 u}{\partial x^2} + \frac{\partial^2 u}{\partial y^2} + \frac{\partial^2 u}{\partial z^2}\right) \tag{4}$$

http://dx.doi.org/10.5772/63532

$$\rho\left(u\frac{\partial v}{\partial x}+v\frac{\partial v}{\partial y}+w\frac{\partial v}{\partial z}\right)=-\frac{\partial p}{\partial y}+\mu\left(\frac{\partial^2 v}{\partial x^2}+\frac{\partial^2 v}{\partial y^2}+\frac{\partial^2 v}{\partial z^2}\right) \tag{5}$$

$$\rho\left(u\frac{\partial w}{\partial x}+v\frac{\partial w}{\partial y}+w\frac{\partial w}{\partial z}\right)=-\frac{\partial p}{\partial z}+\mu\left(\frac{\partial^2 w}{\partial x^2}+\frac{\partial^2 w}{\partial y^2}+\frac{\partial^2 w}{\partial z^2}\right) \tag{6}$$

where $u/v/w$ are velocity components, $x/y/z$ are Cartesian coordinates, ρ is fluid density, p is fluid pressure, μ is viscosity.

Additionally, gas may escape from the lubricant or lubricant may vapour, when the pressure drops to negative value, which means that the fluid film of journal bearings ruptures and a cavitation phenomenon occurs. As it was well known, some numerical models had been developed to describe the cavitation phenomenon, for example, the half-Sommerfeld boundary condition, Reynolds boundary condition and the Jakobsson-Floberg-Olsson (JFO) formulation. In order to consider the generating mechanism of vapour and the transitions between liquid and vapour, the cavitation phenomenon in fluid domain is governed by a phase change model based on pressure change, i.e. phase transitions between liquid and vapour resulting from pressure change.

The transition from liquid phase to vapour phase is triggered when the pressure is less than the saturation vapour pressure, P_{Sat}. All the variables in the governing equations adopt the corresponding value of mixture phase (i.e. liquid phase + vapour phase). The physical properties of the mixture phase are scaled by the liquid volume fraction, f. The liquid volume fraction, f, is defined as the ratio of liquid volume to the total volume (liquid volume + vapour volume). So, the physical properties of mixture phase α are defined as

$$\alpha = f\cdot\alpha_{\mathrm{l}}+(1-f)\cdot\alpha_{\mathrm{v}} \tag{7}$$

The subscripts l and v represent the liquid phase and vapour phase, respectively. As the pressure is higher than the saturation vapour pressure, P_{Sat}, the liquid volume fraction f is equal to 1. As it is well known, the ambient pressure (its absolute value is 1 atm) is usually used to study the cavitation phenomenon in tribological analysis. The saturation vapour pressure, P_{Sat}, is equal to 1 atm in this chapter. When there is a liquid-vapour transition as the pressure changes, mass conservation is satisfied and the mass transfer rate m is to be modelled as

$$\begin{cases} m^{+}=\dfrac{2C_{\mathrm{c}}}{U_{\mathrm{m}}^2 t_{\mathrm{m}}}\cdot(1-f)\cdot\max(0,p-P_{\mathrm{Sat}}) \\ m^{-}=\dfrac{2C_{\mathrm{v}}\rho_{\mathrm{l}}}{U_{\mathrm{m}}^2 t_{\mathrm{m}}\rho_{\mathrm{v}}}\cdot f\cdot\min(0,p-P_{\mathrm{Sat}}) \end{cases} \tag{8}$$

where C_σ, C_v, U_m and t_m are empirical constants based on the mean flow. The superscripts, + and –, represent the phase change from vapour to liquid (condensation) and the phase change from liquid to vapour (vapourisation), respectively.

4. Influences of boundary slip on hydrodynamic journal bearings

4.1. Hydrodynamic journal bearing model

The hydrodynamic journal bearing is presented in **Figure 3**. The journal radius, r, is 25 mm; the bearing width, B, is 25 mm; the radial clearance, c, is 50 μm; and the eccentricity is 0.55. The density of lubricant (water), ρ, is 998.2 kg·m^{-3}, and its viscosity, μ, is 1.003 mPa·s. The thickest and thinnest positions of the lubrication film are located at 90° and 270° in the circumferential direction, respectively. The rotational speed of journal ω is 10^4 rpm, about 1047.2 rad·s^{-1}. The pressures at the two end surfaces of lubricant domain in axial direction are equal to ambient pressure.

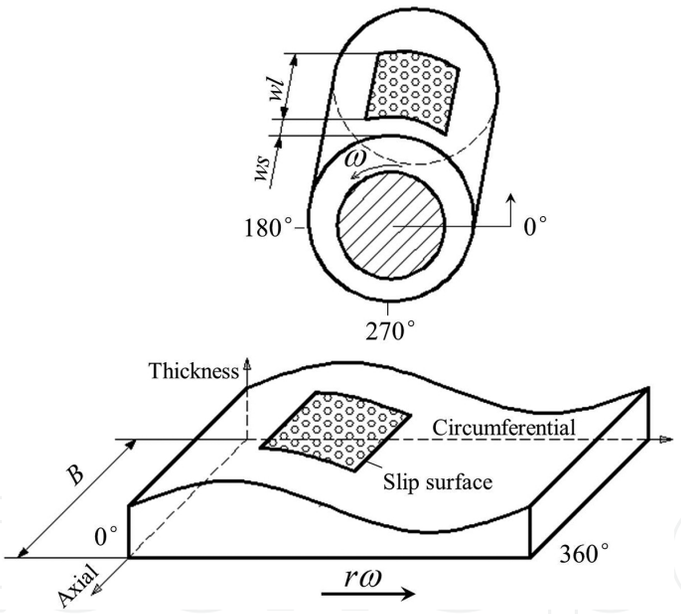

Figure 3. Hydrodynamic journal bearing with a slip surface.

The slip surface is designed on the internal surface of bearing bush, as shown in **Figure 3**. The distance from the bearing end surface to the starting position of slip surface in axial direction is marked as ws. The ratio of ws to the bearing width, B, is defined as the dimensionless slip-surface starting position, WS, i.e. WS = ws/B. And the dimensionless slip-surface width, WL, is defined as the ratio of the slip-surface width, wl, in axial direction to the bearing width, B, i.e. WL = wl/B. The slip intensity model is applied to slip region, and the traditional no-slip boundary condition is applied to other regions.

4.2. Slip intensity's influences

The influences of slip intensity on tribological performance of hydrodynamic journal bearing are investigated first. Two bearing models with different slip surfaces are analysed: one slip surface is located at 160–200° in circumferential direction, the other slip surface is located at 250–260°; their axial location is both defined by WL = 1.0 (which implies WS = 0).

Boundary slip not only could improve the load-carrying capacity of hydrodynamic journal bearing but also could reduce it, which is related to the position of slip surface, as shown in **Figure 4**, and we will analyse in detail later. The load-carrying capacity, w, is obtained from the pressure integral over the journal surface, and the dimensionless load-carrying capacity is defined as $W = w \cdot c^2/(\mu \cdot r^3 \cdot \omega \cdot B)$.

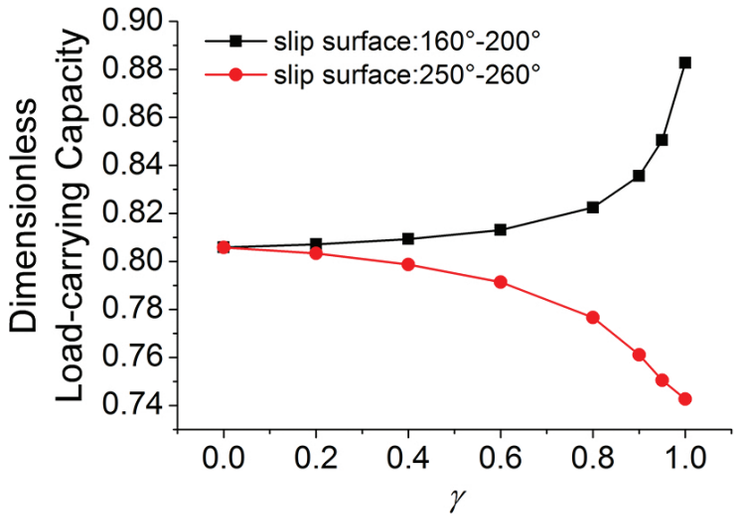

Figure 4. Influences of slip intensity.

If boundary slip could enhance the load-carrying capacity, its beneficial influence increases with the slip intensity, i.e. the value of slip-intensity factor, γ. Otherwise, if boundary slip has adverse effect on load-carrying capacity, its negative influence will also increase with the slip intensity. In a word, the influence of slip intensity is monotonic. For focusing on the influences of the position and size/area of slip surface, a same slip intensity, γ = 1, is utilised in the following analysis.

4.3. Influences of circumferential positions and sizes of slip surfaces

The influences of location and size of slip surface in the circumferential direction on pressure and load-carrying capacity are investigated. In this section, the impacts of location and size of slip surface in axial direction are not taken into account, so the slip region covers the whole internal surface of bearing bush in axial direction. The dimensionless pressure is defined as $P = p \cdot c^2/(\mu \cdot r \cdot \omega \cdot B)$.

4.3.1. Slip surfaces in cavitation zone

The pressure distribution in the medium cross section in axial direction is illustrated in **Figure 5**, for these two situations, namely the size of slip surface is zero and the slip surface is located from 320° to 340°. For this situation, the size of slip surface is zero, i.e. there is no slip surface, and the maximum pressure is located at 234.5°. This pressure peak results from the fluid hydrodynamic action while the lubricant is flowing into a convergence region (bearing bush and journal shaft are not concentric). The hydrodynamic pressure rising zone is located from 94.5° to 234.5°, where $\partial p/\partial\theta > 0$, θ represents the circumferential angle. The pressure drop zone is located from 234.5° to 283.6°, where $\partial p/\partial\theta < 0$. The cavitation zone is located at 0–94.5° and 283.6–360°.

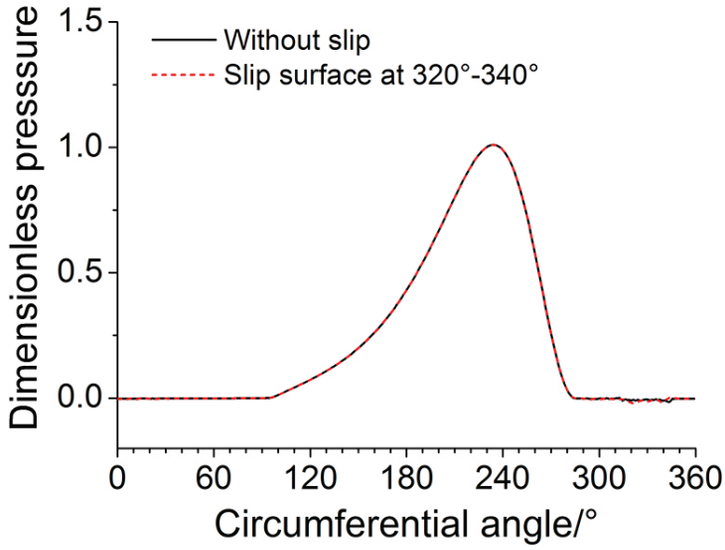

Figure 5. Pressure distribution for without slip surface and slip surface located at 320–340°.

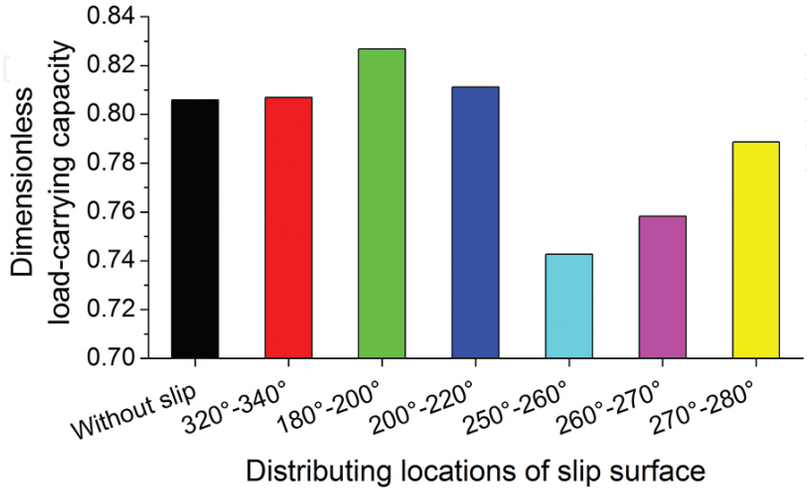

Figure 6. Load-carrying capacity for different slip surfaces.

It can be seen from **Figure 5**, for this situation, the slip surface is located from 320° to 340°, namely it's just located at the cavitation zone, its pressure distribution is the same as that when there is no boundary slip. The difference in load carrying capacity between these two situations is also very small and can be neglected, as shown in **Figure 6**. The reason lies on the pressure in cavitation zone. When fluid pressure drops below the saturation vapour pressure, phase change occurs and liquid is converted into vapour; then the pressure in these vapour regions (cavitation regions) is equal to the saturation vapour pressure. Consequently, if slip surface is located in the cavitation zone, it would have no influence on pressure.

4.3.2. Slip surfaces in pressure rising zone

Pressure distribution along circumferential direction for these three situations, namely there is no slip surface and the slip surface is from 180° to 200° and from 200° to 220°, is presented in **Figure 7**. These three situations all have a pressure peak, which is located at the same position near 234.5°. This pressure peak is induced by the fluid hydrodynamic action when the lubricant flows into a convergence region, because the bearing bush and rotary shaft are not concentric.

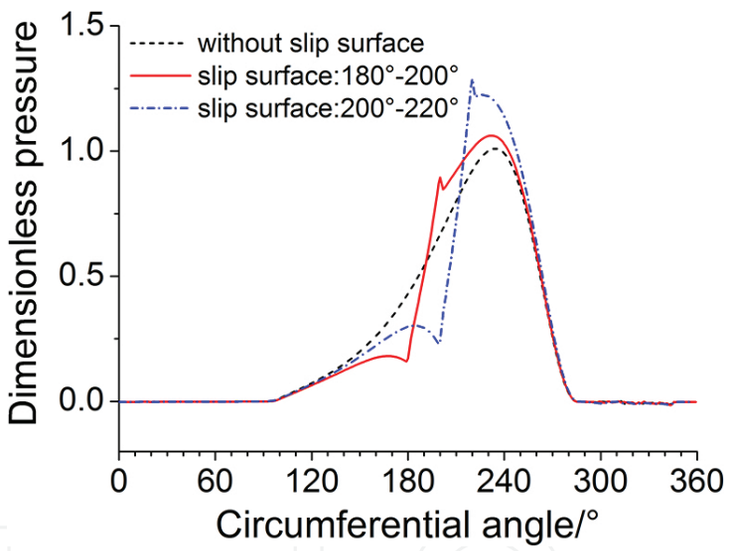

Figure 7. Pressure distribution for slip surfaces located at pressure rising zone.

For these two situations, namely slip surface is located at 180–200° and 200–220°, there is one other pressure peak, which is located at 200° and 220°, respectively. These two additional pressure peaks are just located at the end line of the downstream zone of slip surface, which is induced by slip surface. This is because when the fluid (lubricant) flows from a slip region into a no-slip region, its speed will decrease, i.e. the kinetic energy of lubricant will decrease, and the kinetic energy will transform into pressure energy; thus, the slip surface will produce a fluid hydrodynamic action in its downstream zone.

It can be seen from **Figure 7**, both these two slip situations also have a valley point in the curves of pressure distribution, which are located at 180° and 200°, i.e. the starting positions of slip surfaces; that is, to say that there is a negative fluid hydrodynamic action in the upstream zone

of slip region. These valley points of pressure are induced by slip surface too. This is because when the fluid (lubricant) flows from a no-slip region to a slip region, the speed of fluid increases, i.e. the kinetic energy of lubricant is increased, and the increased part of kinetic energy is transformed from the pressure energy, so the pressure is decreased.

Taking the highest pressure of this case without slip surface, namely the pressure value at 234.5°, as a reference pressure, when the slip surface is located at 180–200°, the value of pressure peak at 200° is about 88.5% of reference pressure and the pressure value at 234.5° is 1.1 times of reference pressure. When the slip surface is located at 200–220°, the value of pressure peak at 220° is about 1.28 times of reference pressure and the pressure value at 234.5° is 1.21 times of reference pressure. Consequently, slip surfaces could enhance fluid hydrodynamic action. Slip surfaces at 180–200° and 200–220° are located at the hydrodynamic pressure rising zone, namely the region from 94.5° to 234.5°. It also can be seen form **Figure 6**, the load-carrying capacities of these two situations, i.e. slip surfaces located at 180–200° and 200–220°, are larger than that without slip surface. These indicate that the fluid hydrodynamic actions produced by boundary slip and convergence structure would promote each other when the slip surface is located in pressure rising zone, and the pressure of lubrication film will increase, and then it also results in an increase in load-carrying capacity.

The pressure distribution for these slip surfaces whose starting positions are fixed at 160° is illustrated in **Figure 8**. Due to the negative fluid hydrodynamic action induced by slip surfaces in their upstream zones, there is a valley value located at 160° for each pressure distribution curve. It can be seen clearly from **Figure 8**, for these three situations that slip surface is located at 160–200°, 160–220° and 160–240°, and the fluid films have ruptured lightly, meaning that a little cavitation phenomenon occurs.

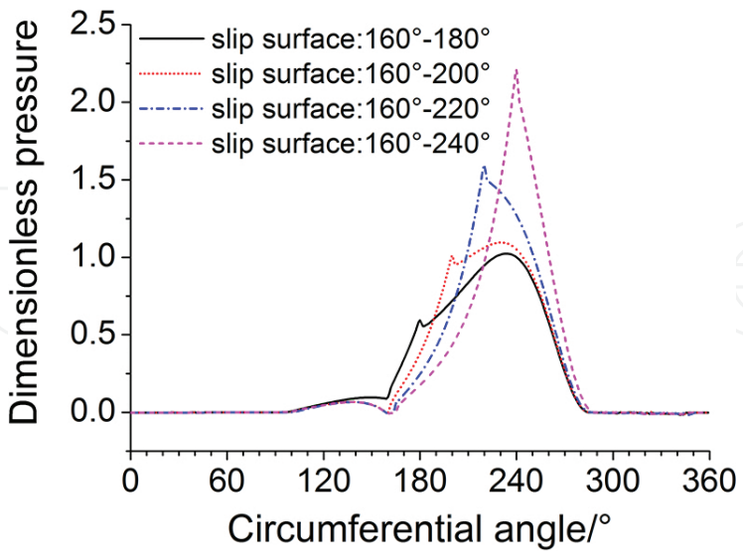

Figure 8. Pressure distribution for slip surfaces starting at 160°.

The pressure distribution curve for slip surface located at 200–220° has two pressure peaks, one located at 220° and the other located at 234.5°; while it has only one pressure peak located

at 220°, for slip surface located at 160–220°. When slip surfaces' end positions are located near 234.5°, the two pressure peaks induced by slip surface and convergence structure, respectively, may merge into a single peak, for example, the slip surfaces located at 160–220° and 160–240°. The size/area of slip surface located at 160–220° is bigger than that located at 200–220°; thus, the fluid hydrodynamic action induced by slip surface located at 160–220° is correspondingly stronger than that for the slip surface located at 200–220°; then, the pressure peak due to slip surface located at 160–220° covers the pressure peak due to convergence structure, while the pressure peak due to slip surface located at 200–220° cannot cover the pressure peak due to convergence structure.

The load-carrying capacity for these slip surfaces whose starting positions are fixed at 160° is illustrated in **Figure 9**, and it shows that the load-carrying capacity increases with the size/area of slip surface. When the end position of slip surface moves from 180° to 240°, correspondingly the circumferential length of slip surface increases from 20° to 80°, and the improving ratio of load-carrying capacity, comparing with the load-carrying capacity without slip surface, increases from 3.2 to 27.9%. It can be concluded that the load-carrying capacity increases with the size/area of slip surface located at the hydrodynamic pressure rising zone.

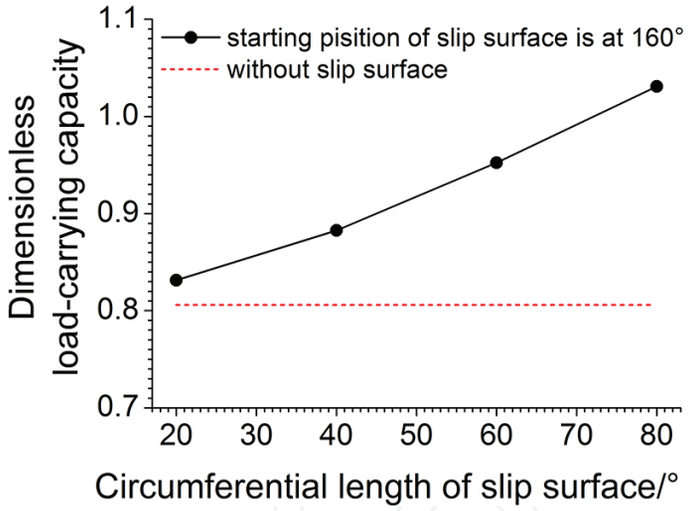

Figure 9. Load-carrying capacity for slip surfaces starting at 160 °.

4.3.3. Slip surfaces in pressure drop zone

The pressure distribution for slip surfaces located at pressure drop zone, namely 250–260°, 260–270° and 270–280°, is shown in **Figure 10**. Due to the negative fluid hydrodynamic action induced by slip surfaces at their upstream zones, these three pressure distribution curves have a valley value located at each starting position of slip surfaces, i.e. at 250°, 260° and 270°. There still is a pressure peak located at each end position of slip surfaces, i.e. at 260°, 270° and 280°. These pressure peaks are induced by slip surfaces. Because these positions of the negative fluid hydrodynamic action induced by slip surfaces located near the high-pressure zone of the fluid hydrodynamic action induced by convergence structure, the fluid hydrodynamic action

induced by convergence structure will be inhibited and its intensity correspondingly becomes much lower. Sometimes, the fluid film at the upstream zone of slip surface will be broken up, for example, for these situations when slip surfaces are located at 260–270° and 270–280°; and it is meant that the cavitation phenomenon is enhanced. This is the reason why the load-carrying capacity for those slip surfaces located at pressure drop zone is smaller than that without slip surface. It can be clearly seen from **Figure 6**, the load-carrying capacity, when slip surface locates at 250–260°, 260–270° and 270–280°, is much smaller compared with that without slip surface.

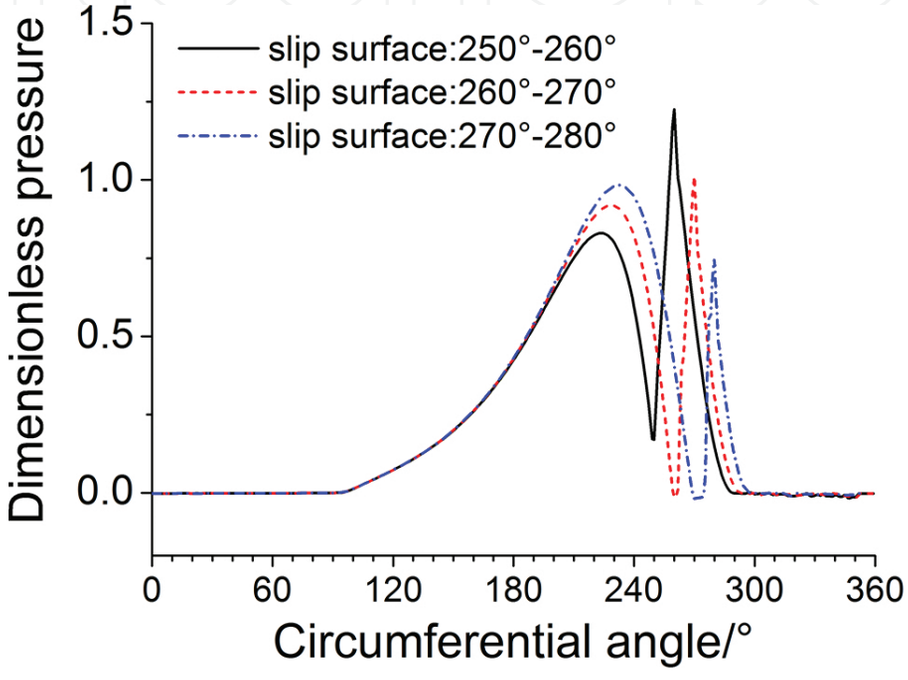

Figure 10. Pressure distribution for slip surfaces located at pressure drop zone.

The pressure distribution for these slip surfaces whose starting positions are fixed at 240° is illustrated in **Figure 11**; these four slip surfaces all are located at the pressure drop zone. Due to the negative fluid hydrodynamic action induced by slip surfaces in their upstream zones, there is a valley value located at 240° for each pressure distribution curve. It can be seen clearly, for these three situations that slip surface located at 240–260°, 240–270° and 240–280°, the fluid films at the upstream zones of slip surfaces have ruptured, meaning that cavitation phenomenon occurs. Because the additional cavitation zones are located at the high-pressure zone of the fluid hydrodynamic action induced by convergence structure, there is an adverse influence on load-carrying capacity. As shown in **Figure 12**, when the starting positions of slip surfaces fix at 240° and their end positions move from 250° to 280°, their load-carrying capacities are all smaller than that without slip surface; as the circumferential length of slip surface increases from 10° to 40°, the decreasing ratio of load-carrying capacity, comparing with the load-carrying capacity without slip surface, increases from 5.9 to 17.0%. It can be concluded that the load-carrying capacity decreases with the size/area of slip surface located at hydrodynamic pressure drop zone.

http://dx.doi.org/10.5772/63532

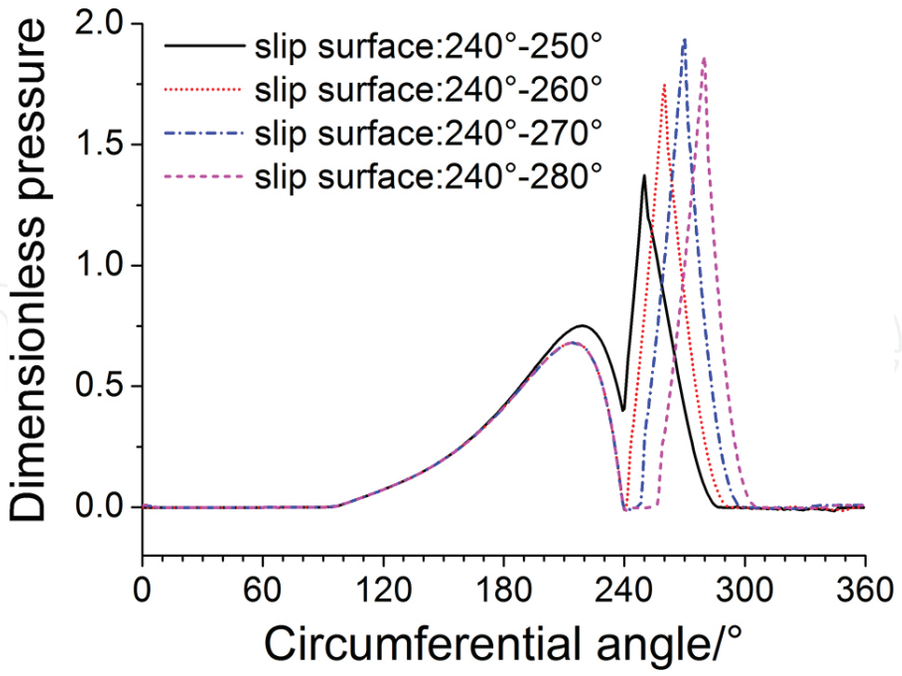

Figure 11. Pressure distribution for slip surfaces starting at 240°.

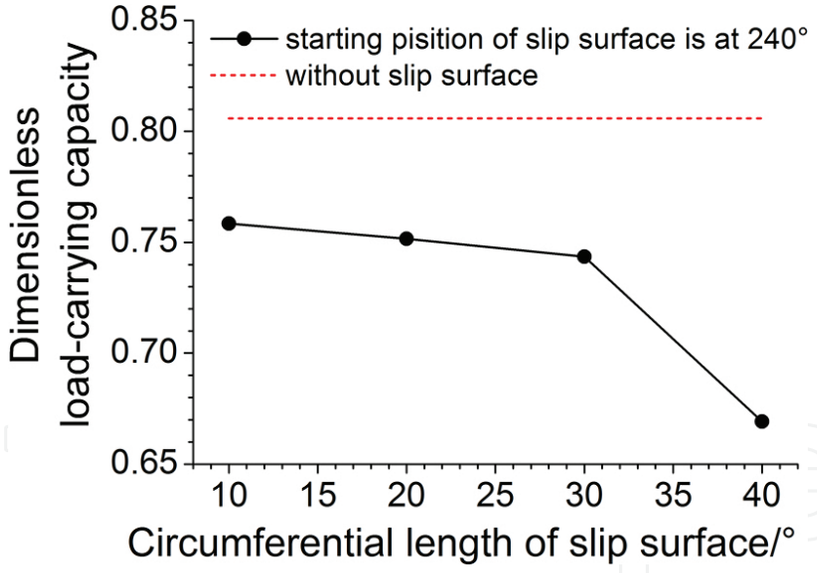

Figure 12. Load-carrying capacity for slip surfaces starting at 240°.

4.4. Influences of axial positions and sizes of slip surfaces

The influences of position and size of slip surface in the axial direction on load-carrying capacity are investigated in the following section. To focus on the impact of the parameters of slip surface in axial direction, the positions and sizes of slip surfaces in the circumferential direction are kept unchanged.

The three-dimensional distribution of local pressure for slip surfaces with different positions and areas in axial direction is illustrated in **Figure 13**; all these slip surfaces are located at 100–120° in the circumferential direction. The pressure peaks and valleys in the downstream and upstream zones of slip surfaces, respectively, are very obvious. It can be seen from **Figure 13 (a), (c)** and **(e)**, namely cases for slip surfaces with a same size (WL = 0.2), if the axial widths of slip surfaces are equal, the widths of pressure peak zones, as well as pressure valley zones, also kept equal, even though the axial positions of slip surfaces are different. As shown in **Figure 13 (b), (d)** and **(f)**, namely cases for slip surfaces with a same starting position (WS = 0.3), as the dimensionless slip-surface width increase from 0.3 to 0.5, the widths/sizes of pressure peak and valley zones still increase correspondingly. It can be concluded that the sizes of pressure peak and pressure valley zones induced by slip surfaces increase with the axial sizes of slip surfaces, but have no relationship with the axial positions of slip surfaces.

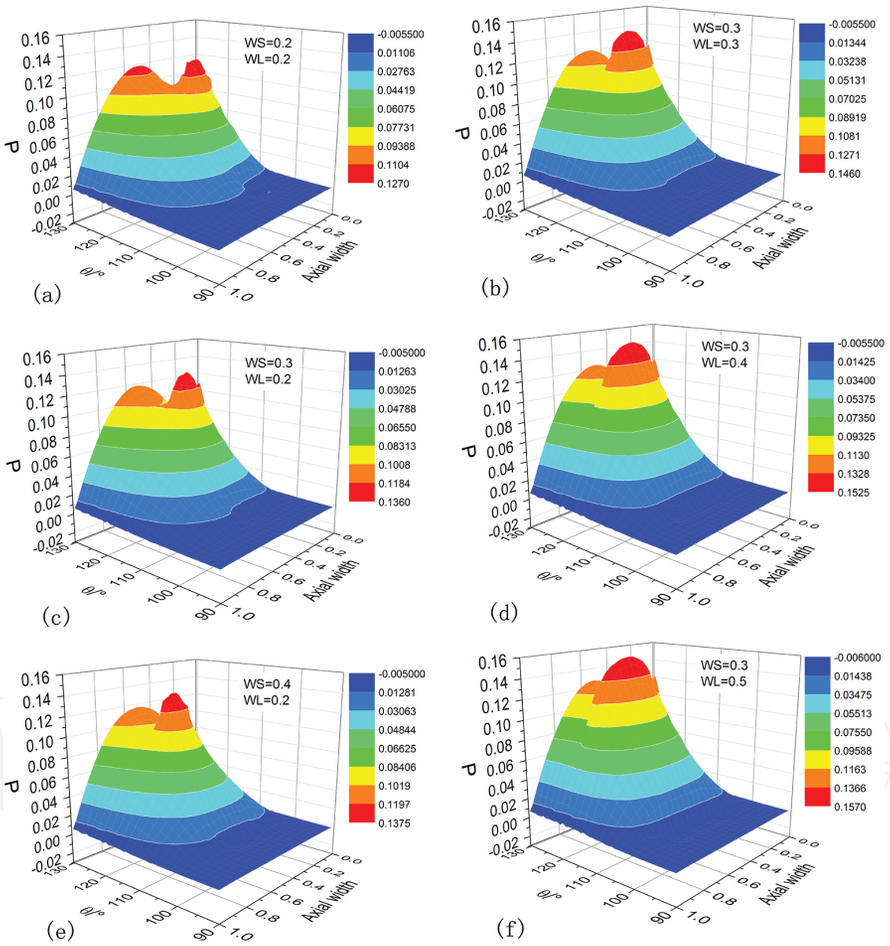

Figure 13. Three-dimensional distribution of local pressure for different slip surfaces.

The load-carrying capacity for slip surfaces with different positions and sizes in the axial direction is presented in **Figure 14**. These slip surfaces are located at 160–180° in the circumferential direction. The load-carrying capacity increases with the axial size of slip surface. For the case that the dimensionless starting position of slip surface, WS, is equal to 0.2, there is an

increase of 3.8% in the load-carrying capacity when the dimensionless slip-surface width, WL, increases from 0.1 to 0.6.

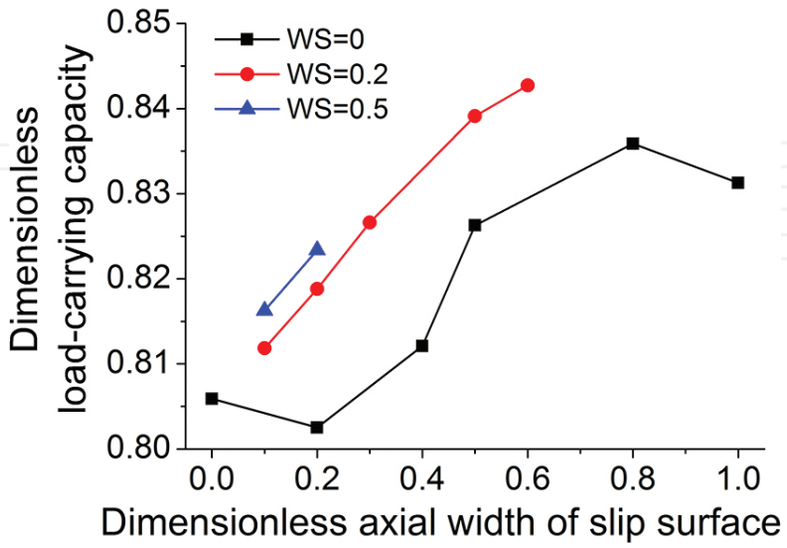

Figure 14. Load carrying-capacity for different slip surfaces.

The distribution curve of load-carrying capacity for WS = 0.5 lies above the curve for WS = 0.2, and the curve for WS = 0.2 lies above the curve for WS = 0, as shown in **Figure 14**. When the axial width of slip surface keeps unchanged (WS = 0.2), moving the starting position of slip surface from outlet (WS = 0) to bearing centre (WS = 0.5), there is an increase of 1.7% in load-carrying capacity. This indicates that the enhanced impacts of slip surfaces on load-carrying capacity are much stronger if the slip surface is located near the bearing centre, under the same axial width.

It can be seen from **Figure 14** the load-carrying capacity for the situation that WS = 0 and WL = 0.2 is smaller than that when WS = 0 and WL = 0. The load-carrying capacity for the situation WS = 0 and WL = 1.0 is also smaller than that when WS = 0 and WL = 0.8. When WS =0, the starting position of slip surface is just located at the bearing axial outlet. When WS = 0 and WL = 1.0, both the starting and the end positions of slip surface are just located at the bearing axial outlet. This situation, WS = 0 and WL = 0, means the size of slip surface is 0, namely there is no slip surface in bearing bush surface. Thus, it can be concluded that slip surface located at bearing axial outlet has an adverse effect on load-carrying capacity.

5. Influences of boundary slip on hybrid journal bearings

5.1. Hybrid journal bearing model

The hybrid journal bearing with two rectangular recesses is presented in **Figure 15**. The journal radius, r, is 25 mm; the bearing width, B, is 25 mm; the radial clearance, c, is 50 μm; and the eccentricity is 0.55. The density of lubricant (water), ρ, is 998.2 kg·m^{-3}, and its viscosity, μ, is

1.003 mPa·s. The axial width of rectangular recess is 15 mm, its circumferential length is 30°, and its radial depth is 50 μm. These two rectangular recesses are located at 165–195° and 345–360°(0°)–15° along the circumference. The rotational speed of journal ω is 10^4 rpm, about 1047.2 rad·s^{-1}. The supply pressure is 15 kPa. The pressures at the two end surfaces of lubricant domain in axial direction are equal to ambient pressure. The thickest and thinnest positions of the lubrication film are located at 130° and 310° in the circumferential direction, respectively, seeing **Figure 15 (c)** which illustrates the thickness distribution and pressure distribution without slip surface.

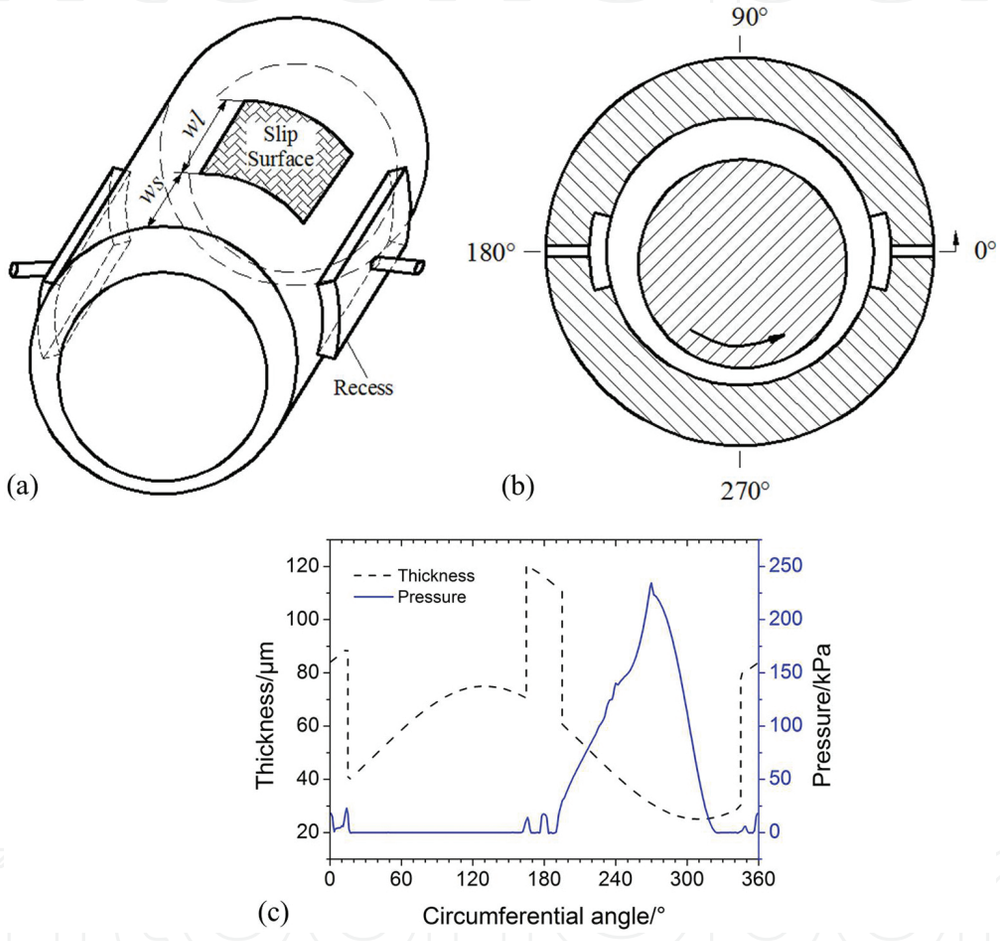

Figure 15. Schematic diagram of hybrid journal bearing: (a) complete view, (b) medium cross section in axial direction, (c) lubrication-film thickness and pressure distribution.

The slip surface is designed on the internal surface of bearing bush, as shown in **Figure 15 (a)**. The distance from the bearing end surface to the starting position of slip surface in axial direction is marked as *ws*. The ratio of *ws* to the bearing width, *B*, is defined as the dimensionless slip-surface starting position, WS, i.e. WS = *ws*/*B*. And the dimensionless slip-surface width, WL, is defined as the ratio of the slip-surface width, *wl*, in axial direction to the bearing width, *B*, i.e. WL=*wl*/*B*. The slip intensity model is applied to slip region, and the traditional no-slip boundary condition is applied to other regions.

5.2. Slip intensity's influences

The influences of slip intensity on tribological performance of hydrodynamic journal bearing are investigated first. Two bearing models with different slip surfaces are analysed: one slip surface is located at 210–240° in circumferential direction, the other slip surface is located at 270–300°; their axial location is both defined by WL = 1.0 (which implies WS = 0).

Boundary slip not only could improve the load-carrying capacity of hydrodynamic journal bearing but also could reduce it, which is related to the position of slip surface, as shown in **Figure 16**. This phenomenon is similar with that for hydrodynamic journal bearings with slip surfaces and we will analyse in detail later.

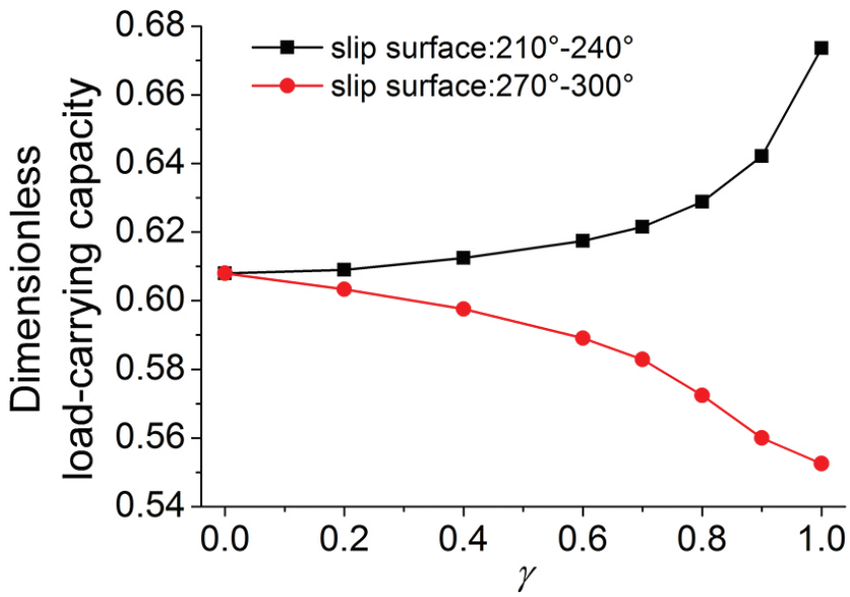

Figure 16. Influences of slip intensity.

If the boundary slip could enhance the load-carrying capacity, its beneficial influence increases with the slip intensity, i.e. the value of slip-intensity factor, γ. Otherwise, if the boundary slip has adverse effect on load-carrying capacity, its negative influence will increase with the slip intensity. In a word, the influence of slip intensity is monotonic. For focusing on the influences of the position and size/area of slip surface, a same slip intensity, $\gamma = 1$, is utilised in the following analysis.

5.3. Influences of circumferential positions and sizes of slip surfaces

The influences of location and size of slip surface in the circumferential direction on pressure and load-carrying capacity are investigated. In this section, the impacts of location and size of slip surface in axial direction are not taken into account, so the slip region covers the whole internal surface of bearing bush in axial direction.

5.3.1. Slip surfaces in cavitation zone

The pressure distribution in the medium cross section in axial direction is illustrated in **Figure 17**, for these two situations, namely the size of slip surface is zero and the slip surface is located from 60° to 90°. For this situation, the size of slip surface is zero, i.e. there is no slip surface, and the maximum pressure is about located at 270°. This pressure peak results from the fluid hydrodynamic action while the lubricant is flowing into a convergence region (bearing bush and journal shaft are not concentric). The hydrodynamic pressure rising zone is located from 195° to 270°, where $\partial p/\partial\theta > 0$, θ represents the circumferential angle. The pressure drop zone is located from 270° to 323°, where $\partial p/\partial\theta < 0$. The cavitation zone is located at 15–165° and 323–345°.

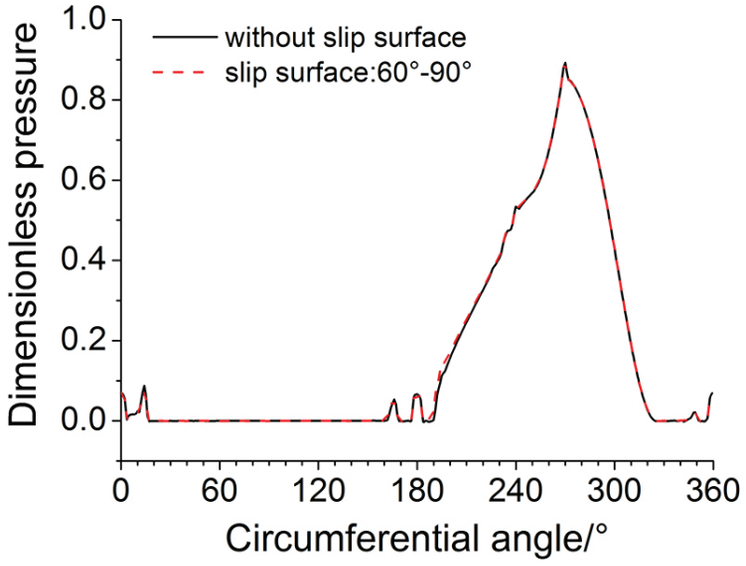

Figure 17. Pressure distribution for without slip surface and slip surface located at 60–90°.

It can be seen from **Figure 17**, for this situation, the slip surface is located from 60° to 90°, namely it's just located at the cavitation zone, its pressure distribution is the same as that when there is no boundary slip. The reason lies on the pressure in cavitation zone. When fluid pressure drops below the saturation vapour pressure, phase change occurs and liquid is converted into vapour, then the pressure in these vapour regions (cavitation regions) is equal to the saturation vapour pressure. Consequently, if slip surface is located in the cavitation zone, it would have no influence on pressure. Their difference in load-carrying capacity is also very small and can be neglected.

5.3.2. Slip surfaces in pressure rising zone

The pressure distribution in the medium cross section in axial direction is illustrated in **Figure 18**, for these four situations, namely the size of slip surface is zero and the slip surface located at 240–270°, 210–270° and 195–270°. These three slip surfaces, namely located at 240–270°, 210–270° and 195–270°, are located in the pressure rising zone.

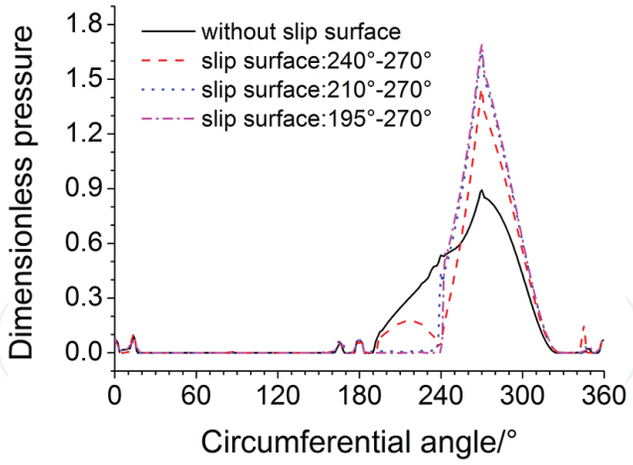

Figure 18. Pressure distribution for slip surfaces located in pressure rising zone.

For the three situations, namely when the slip surfaces are located at 240–270°, 210–270° and 195–270°, i.e. the end positions of slip surfaces are fixed at 270°, their maximum pressures are all higher than that without slip surface. These slip surfaces could enhance the fluid hydrodynamic action. The reason is that when the lubricant flows from a slip surface into a non-slip surface, its speed will decrease, i.e. the kinetic energy of the lubricant will decrease and then the kinetic energy will transform into pressure energy; as a result, the slip surface will produce a fluid hydrodynamic action in its downstream zone. The position of maximum pressure is just located at the end line of the downstream zone of the slip surface, as also clearly shown in **Figure 20**. Thus, the load-carrying capacity increases with the size of slip surface in the pressure rising zone, as shown in **Figure 19**.

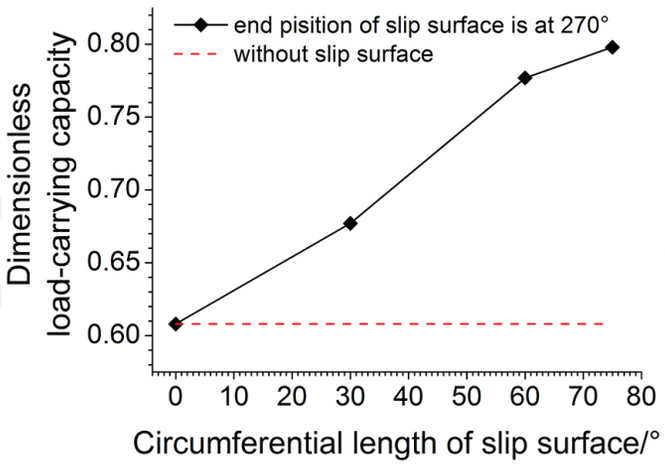

Figure 19. Load-carrying capacity for slip surfaces located in pressure rising zone.

Comparing with the situation without the slip surface, there is an increase of 11.4% in the load-carrying capacity when the slip surface is located from 240–270°. When the starting position of slip surface moves from 240° to 195°, the size of slip surface correspondingly increases from

30° to 75°, and the rate of load-carrying capacity comparing with the case without slip surface increases to 31.3%.

Figure 18 also shows that there is a negative fluid hydrodynamic action in the upstream zone of slip surface, indicating that there is a decrease in pressure. Because when the lubricant flows from a non-slip surface to a slip surface, the speed of fluid increases, i.e. the kinetic energy of the lubricant is increased, and the increased part of kinetic energy is transformed from the pressure energy, thereby decreasing the pressure. Thus, in the upstream zone of slip surface, the fluid hydrodynamic action induced by convergence structure will break down. In particular, when the slip surface is located in the pressure drop zone, the high-pressure zone induced by convergence structure, namely the main load-carrying zone, maybe broken up by the negative fluid hydrodynamic action due to slip surface, and the load-carrying capacity also may decrease, which will be discussed in the following section.

5.3.3. Slip surfaces in pressure drop zone

Pressure distribution and load-carrying capacity for slip surfaces located in pressure drop zone are presented in **Figures 20** and **21**, respectively. **Figure 21** indicates that the load-carrying capacity decreases with increasing size of the slip regions in the pressure drop zone. These four slip regions have the same starting location, located at 270°, and their end locations are located at 300°, 305°, 310° and 315°. Compared with the situation without slip surface, there is a decrease of 9.1% in load-carrying capacity when the slip surface is from 270° to 300°. When extending the end position of slip surface to 315°, the load-carrying capacity has a further decrease and its decrease rate, comparing with the case without slip surface, increases to 57.2%.

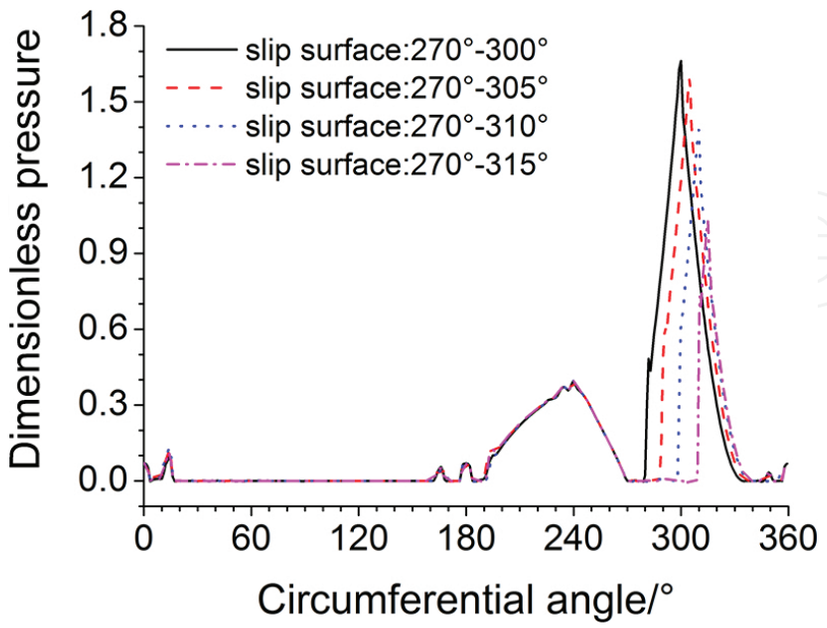

Figure 20. Pressure distribution for slip surfaces located in pressure drop zone.

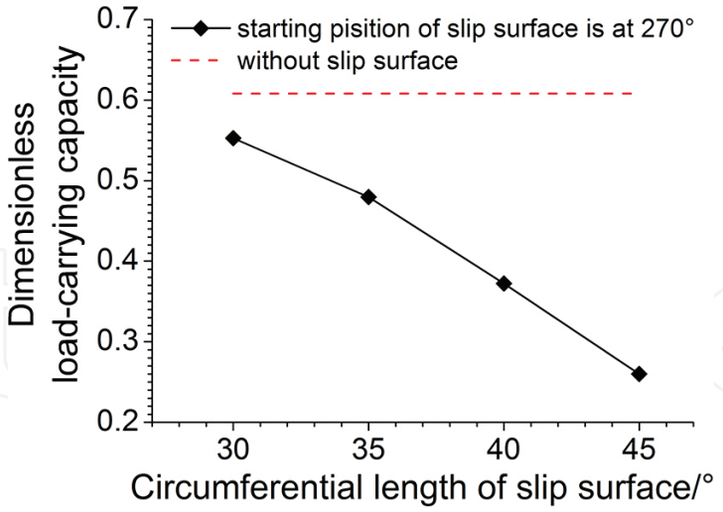

Figure 21. Load-carrying capacity for slip surfaces located in pressure drop zone.

5.4. Influences of axial positions and sizes of slip surfaces

The influences of position and size of slip surface in the axial direction on load-carrying capacity are investigated in the following section. To focus on the impact of the parameters of slip surface in axial direction, the positions and sizes of slip surfaces in the circumferential direction are kept unchanged, and these slip surfaces are located from 210° to 240°. The load-carrying capacity for slip surfaces with different positions and sizes in the axial direction is presented in **Figure 22**. The load-carrying capacity increases with the axial size of slip surface. For the case that the dimensionless starting position of slip surface, WS, is equal to 0.15, there is an increase of 8.4% in the load-carrying capacity when the dimensionless slip-surface width, WL, increases from 0.25 to 0.7.

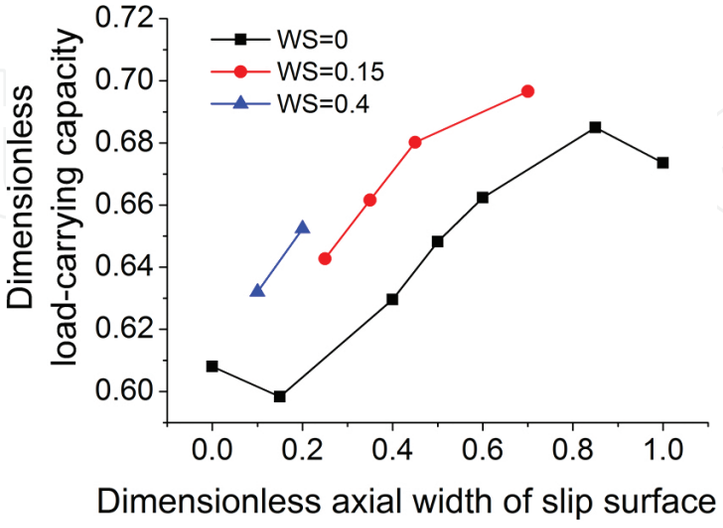

Figure 22. Load carrying-capacity for different slip surfaces.

The distribution curve of load-carrying capacity for WS = 0.4 lies above the curve for WS = 0.15, and the curve for WS = 0.15 lies above the curve for WS = 0, as shown in **Figure 22**. When WS = 0.4 and WL = 0.2, there is an increase of 3.6% in load carrying-capacity compared with this situation as WS = 0.0 and WL = 0.4; although the axial area of the former slip surface is smaller than the latter, the former slip surface is located much more closely to the bearing centre. This indicates that the enhanced impacts of slip surfaces on load carrying-capacity are much stronger if the slip surface is located near the bearing centre, under the same axial width.

It can be seen from **Figure 22**, the load-carrying capacity for the situation that WS = 0 and WL = 0.15 is smaller than that when WS = 0 and WL = 0. The load-carrying capacity for the situation WS = 0 and WL = 1.0 is also smaller than that when WS = 0 and WL = 0.85. When WS = 0, the starting position of slip surface is just located at the bearing axial outlet. When WS = 0 and WL =1.0, both the starting and the end positions of slip surface are just located at the bearing axial outlet. This situation, WS = 0 and WL = 0, means the size of slip surface is 0, namely there is no slip surface in bearing bush surface. Thus, it can be concluded that slip surface located at bearing axial outlet has an adverse effect on load-carrying capacity.

6. Conclusions

Boundary slip has complex influences on the tribological performances of journal bearings, including hydrodynamic and hybrid journal bearings. The impact laws of slip surfaces on journal bearings can be concluded as follows:

1. Boundary slip could produce a fluid hydrodynamic action in the downstream zone of the slip surface, and also could result in a negative fluid hydrodynamic action in the upstream zone of slip surface.

2. These two fluid hydrodynamic actions induced by boundary slip and convergence structure, respectively, may promote each other, when the slip surface is located in the pressure rising zone. In this moment, boundary slip has a beneficial influence and will improve load-carrying capacity, and the load-carrying capacity increases with the size/area of slip surface.

3. The negative fluid hydrodynamic action induced by boundary slip would damage the fluid hydrodynamic action produced by convergence structure, when the slip surface is located in the pressure drop zone. In this case, the boundary slip has an adverse influence, and the load-carrying capacity decreases with the size of slip surface.

4. Due to the pressure condition in cavitation zone, when the slip surface is located in cavitation zone, the boundary slip has no influence on the pressure distribution and load-carrying capacity of journal bearings.

5. The slip surface near the bearing centre in the axial direction has a much stronger influence on the enhancement of the load-carrying capacity.

6. The slip surface located at bearing outlet has an adverse influence on load-carrying capacity.

In summary, unreasonable design of slip surfaces not only cannot improve the tribological performances of journal bearings, including hydrodynamic journal bearings and hybrid journal bearings, but they also have adverse influences and would result in a decrease in load-carrying capacity. These results in this chapter can be a design criterion for the design of slip surfaces in journal bearings.

Author details

Qiyin Lin[1,2*], Baotong Li[2,3] and Hong Zhao[1,2,3]

*Address all correspondence to: qiyinlin88@gmail.com

1 Fuli School of Food Equipment Engineering and Science, Xi'an Jiaotong University, Xi'an, China

2 State Key Laboratory for Manufacturing Systems Engineering, Xi'an Jiaotong University, Xi'an, China

3 School of Mechanical Engineering, Xi'an Jiaotong University, Xi'an, China

References

[1] Jonathan P. Rothstein. Slip on superhydrophobic surfaces. Annual Review of Fluid Mechanics. 2010;42:89–109. DOI: 10.1146/annurev-fluid-121108-145558

[2] Bharat B, Yuliang W, Abdelhamid M. Boundary slip study on hydrophilic, hydrophobic, and superhydrophobic surfaces with dynamic atomic force microscopy. Langmuir. 2009;25(14):8117–8121. DOI: 10.1021/la900612s

[3] Hugh S, Steve G. Equation for slip of simple liquids at smooth solid surfaces. Langmuir. 2003;19(12):5065–5071. DOI: 10.1021/la034123j

[4] H A Spikes. The half-wetted bearing. Part 1: Extended Reynolds equation. Proceedings of the Institution of Mechanical Engineers, Part J: Journal of Engineering Tribology. 2003;217(1):1–14. DOI: 10.1243/135065003321164758

[5] Richard F. Salant, Alicia E. Fortier. Numerical analysis of a slider bearing with a heterogeneous slip/no-slip surface. Tribology Transactions. 2004;47(3):328–334. DOI: 10.1080/05698190490455348

[6] Cho-Yun Y, Cho-Yu Y, Cheng-Kuo S, Chih-Yung H. Design of slip boundary produced by a lotus structure applied to a hydrostatic bearing. Tribology Letters. 2014;55(1):55–64. DOI: 10.1007/s11249-014-0331-2

[7] Aurelian F, Patrick M, Mohamed H. Wall slip effects in (elasto) hydrodynamic journal bearings. Tribology International. 2011;44(7–8):868–877. DOI: 10.1016/j.triboint.2011.03.003

[8] Qiyin L, Zhengying W, Ning W, Wei C. Effects of large-area textured/slip surface on slider bearing. Journal of the Balkan Tribological Association. 2015;21(1):12–23.

[9] Qiyin L, Zhengying W, Ning W, Wei C. Effect of large-area texture/slip surface on journal bearing considering cavitation. Industrial Lubrication and Tribology. 2015;67(3):216–226. DOI: 10.1108/ILT-05-2013-0055

[10] Yongbin Z. A tilted pad thrust slider bearing improved by the boundary slippage. Meccanica. 2013;48:769–781. DOI: 10.1007/s11012-012-9630-6

[11] Qiyin L, Zhengying W, Yubin Z, Ning W. Effects of the slip surface on the tribological performances of high-speed hybrid journal bearings. Proceedings of the Institution of Mechanical Engineers, Part J: Journal of Engineering Tribology. Forthcoming. DOI: 10.1177/1350650116630202

[12] Qiyin L, Baotong L. Comparison of the influences of surface texture and boundary slip on tribological performances. Mathematical Problems in Engineering. 2015;2015:126824. DOI: 10.1155/2015/126824